

# Suppression of coherent errors in Cross-Resonance gates via recursive DRAG

Boxi Li,<sup>1, 2,\*</sup> Tommaso Calarco,<sup>1, 2, 3</sup> and Felix Motzoi<sup>1, †</sup>

<sup>1</sup>*Forschungszentrum Jülich, Institute of Quantum Control (PGI-8), D-52425 Jülich, Germany*

<sup>2</sup>*Institute for Theoretical Physics, University of Cologne, D-50937 Cologne, Germany*

<sup>3</sup>*Dipartimento di Fisica e Astronomia, Università di Bologna, 40127 Bologna, Italy*

The high-precision control of quantum logical operations is a prerequisite to increasing circuit depths in quantum processors, implementing useful quantum algorithms, and reaching fault-tolerant scalable architectures. A ubiquitous approach used for entangling gates has been all-microwave control of superconducting qubits, primarily using the Cross-Resonance two-qubit gate; however, fidelities are still limited by control imperfections. Here, we derive an analytical method that significantly improves fidelities in Cross-Resonance gates, suppressing both the three off-resonant transitions on the control qubit and unwanted two-qubit rotation operators. This reduces the total coherent errors by one to three orders of magnitude across all parameter regimes studied. Our approach uses a simple recursive composition of DRAG pulses derived for each spurious coupling in the corresponding two-level subspace and a correction tone applied resonantly on the target qubit, requiring no additional control hardware overhead.

Superconducting qubits have experienced significant improvement in the last decade, reaching the error correction threshold [1, 2] and been used to study nontrivial quantum phenomena [3, 4]. Nonetheless, due to the presence of spurious couplings and weak non-linearity [5, 6], control errors such as cross-talk and leakage are still significant bottlenecks, especially for multi-qubit operations [7]. These imperfections may lead to correlated errors that spread in the qubit lattice, sabotaging quantum error correction [8], also making error mitigation and benchmarking more challenging [9–12]. To really maintain the coherence of the dynamics, it is necessary to design better control schemes based on the knowledge of the system dynamics.

The Cross-Resonance (CR) gate is one of the most widely used two-qubit entangling gates for superconducting qubits, using microwave controls and avoiding noisy flux lines [6, 13–16]. It has been employed to implement high-quality circuits, parity measurement and state preparation [17–19]. Despite the progress, various coherent errors still bottleneck the gate performance, including off-resonant transitions introduced by the drive [20–22] and unwanted effective dynamics in the qubits’ subspace [21, 23, 24] (see Fig. 1a and Fig. 1b). Various schemes have been proposed to suppress the error in the latter category [16, 25–28], while the former is often only indirectly addressed by prolonging the pulse ramping time.

For the CR gate, the off-resonant transition errors are especially problematic for the straddling regime, needed for fast entanglement [21], where the qubit-qubit detuning is smaller than their anharmonicities. The error transitions are non-negligible among all the three lowest levels [24]. In this case, the first-order DRAG (Derivative Removal by Adiabatic Gate) [29–32] pulse proportional to the first derivative of the control pulse only provides a limited improvement, even if a scale factor is numerically optimized as in [20], having to compromise between which transitions are excited. More generally, this prob-

lem is not only relevant to CR gates, but also exists in other off-resonant drive schemes, such as microwave-activated gates [33–36], suppression of quantum cross-talk and leakage [31, 37–39], including ZZ cross-talk.

Concerning methods to suppress the errors, various techniques have been tested to deliver more performant pulses: Several numerical control algorithms have been used [40–42], but complexity in the pulse shapes and in the usage of the Hilbert space has resulted in poor transferability from model to experiment. Instead, analytical pulse shaping has been the main driver of progress [16], making fast implementation and calibration possible. Nonetheless, much room remains for improvement as the simplicity of the pulses has also limited their fidelity, not coming close to the performance of analytical pulse shapes standard for single-qubit gates [29–31].

In this work, we develop a recursive DRAG method to suppress all relevant error transitions simultaneously. In each step of the recursion, we only focus on suppressing single-error dynamics on the relevant two-level subspace. In this subspace, an exact time-dependent frame transformation may be derived, as well as an expression for the new control pulse. The recursive structure avoids unnecessary expansions and allows one to selectively target all the possible dominant errors across different parameter regimes. Thus, in the experimentally relevant regimes, we find that a simple composition of recursive DRAG pulses provides dramatic suppression of relevant transition errors. We also show the suppression of the remaining multi-qubit rotation-axis errors pulling one out of the  $ZX$  rotation subspace through an additional DRAG-like correction tone applied on the target qubit. An overview of the derived pulse schemes is shown in Fig. 1c and Fig. 1d.

*Suppressing control-qubit transitions* – We start explaining the method with a generic two-level system

$$\hat{H} = \Delta \hat{\Pi}_j + g(t) \frac{\hat{\sigma}_{jk}^+}{2} + g^*(t) \frac{\hat{\sigma}_{kj}^+}{2} \quad (1)$$

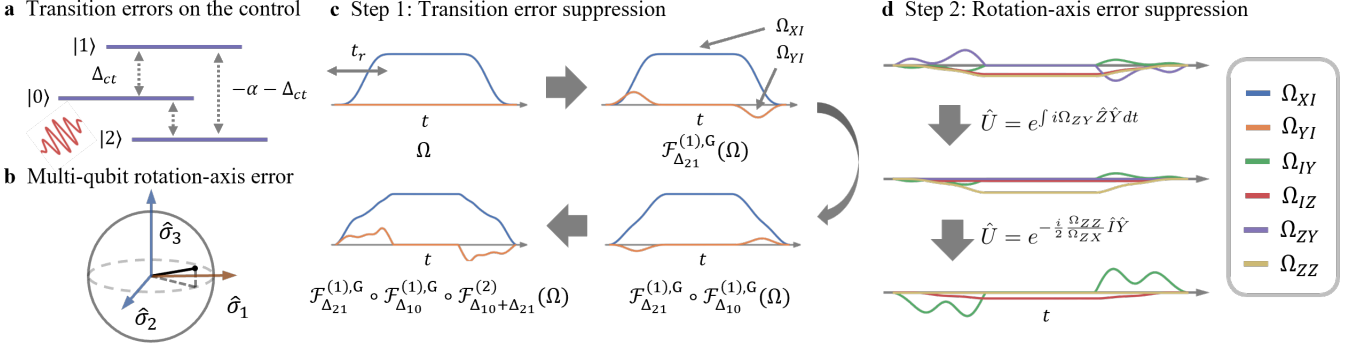


FIG. 1. **a:** Transition errors in the rotating frame for a transmon qubit driven off-resonantly, with  $\Delta_{ct}$  the qubit-qubit detuning and  $\alpha$  the anharmonicity. **b:** rotation-axis errors of the CR gate. The three axes  $\{\hat{\sigma}_1, \hat{\sigma}_2, \hat{\sigma}_3\}$  represent either  $\{\hat{\sigma}_{ZX}, \hat{\sigma}_{ZY}, \hat{\sigma}_{ZZ}\}$  or  $\{\hat{\sigma}_{IX}, \hat{\sigma}_{IY}, \hat{\sigma}_{IZ}\}$ . The Hamiltonians  $ZX$  and  $IX$  (brown) commute and are defined as the ideal dynamics, while the others are considered errors (blue). **c:** Schematic illustration of the recursively-defined CR pulse shapes that suppress different error transitions on the control transmon. **d:** Schematic illustration of different rotation-axis errors in the effective frame during the CR operation, and the transformations of the error terms. The remaining  $IY$  and  $IZ$  errors are compensated for by a  $Y$  drive on the target qubit and the detuning of the CR drive.

where  $\hat{\Pi}_j = |j\rangle\langle j|$  and  $\hat{\sigma}_{jk}^+ = |k\rangle\langle j|$ ,  $g(t)$  denotes the coupling strength between the two levels. In the following, we omit the explicit time dependence on  $t$  for ease of notation. In general,  $g$  could take the (perturbative) form of an  $n$ -photon interaction,  $\frac{\Omega^n}{\Delta_{\text{eff}}^{n-1}}$ , where  $\Delta_{\text{eff}}$  is an effective energy gap and  $\Omega$  the drive strength. In particular, if  $\Omega$  denotes the CR drive strength on the control qubit, with  $n = 1$ , it describes the transition  $|0\rangle \leftrightarrow |1\rangle$  (or  $|1\rangle \leftrightarrow |2\rangle$ ) and with  $n = 2$  the two-photon transition  $|0\rangle \leftrightarrow |2\rangle$ .

The goal is to suppress the undesired transition introduced by the coupling  $g$ . If  $g \ll \Delta$ , we perform a perturbative expansion with the antihermitian generator  $\hat{S}(\tilde{g}) = \frac{\tilde{g}}{2\Delta} \hat{\sigma}_{jk}^+ - h.c.$  and obtain under the transformation  $\hat{H}'(g) = \hat{U}(\tilde{g}) \hat{H}(g) \hat{U}^\dagger(\tilde{g}) + i\dot{\hat{U}}(\tilde{g}) \hat{U}^\dagger(\tilde{g})$  with  $\hat{U}(\tilde{g}) = e^{\hat{S}(\tilde{g})}$ ,

$$\begin{aligned} \hat{H}'(g) &= i\dot{\hat{S}}(\tilde{g}) + \hat{H}(g) + [\epsilon\hat{S}(\tilde{g}), \hat{H}(g)] + \dots \\ &= \Delta\hat{\Pi}_j + \left[ g - \tilde{g} + i\frac{d}{dt}\frac{\tilde{g}}{\Delta} \right] \frac{\hat{\sigma}_{jk}^+}{2} + h.c. + \mathcal{O}(\epsilon^2). \end{aligned} \quad (2)$$

We deliberately distinguish between  $g$ , the actual physical coupling, and  $\tilde{g}$ , which is used to define the generator  $\hat{S}$  that diagonalizes the Hamiltonian. For a time-dependent  $g$ , to suppress the transition, we require

$$g = \tilde{g} - i\frac{d}{dt}\frac{\tilde{g}}{\Delta}. \quad (3)$$

The above equation also provides an alternative interpretation: Transition-less evolution is possible if we find a (perturbative, counter-diabatic) control  $g(t)$  by choosing any continuous function  $\tilde{g}(t)$  and making sure that  $\hat{S}(\tilde{g})$  is zero at the beginning and at the end of the time evolution [43–46]. Thus, Eq. (3) provides a substitution rule to obtain a time-modulated coupling  $g(t)$  with the

transition between the two levels suppressed. If the coupling describes an  $n$  photon interaction generated by a drive  $\Omega$ , i.e.,  $g = \frac{\Omega^n}{\Delta_{\text{eff}}^{n-1}}$  with a constant  $\Delta_{\text{eff}}$ , we obtain

$$\Omega = \mathcal{F}_\Delta^{(n)}(\tilde{\Omega}) := \left( \tilde{\Omega}^n - i\frac{d}{dt}\frac{\tilde{\Omega}^n}{\Delta} \right)^{\frac{1}{n}}. \quad (4)$$

Here, we choose  $\tilde{g} = \frac{\tilde{\Omega}^n}{\Delta_{\text{eff}}^{n-1}}$  to keep the notation intuitive. The fractional exponent is defined for complex numbers and needs to ensure the continuity of  $\Omega$  as a function of  $t$ . For  $n = 1$  this gives the familiar result of the first-order DRAG expansion [31].

More generally, a two-level Hamiltonian (or subspace), in Eq. (1), is diagonalized exactly by the unitary transformation [47]

$$\hat{U} = \begin{pmatrix} \cos\left(\frac{\theta}{2}\right) & e^{-i\phi}\sin\left(\frac{\theta}{2}\right) \\ -e^{i\phi}\sin\left(\frac{\theta}{2}\right) & \cos\left(\frac{\theta}{2}\right) \end{pmatrix}, \quad (5)$$

resulting in an exact substitution rule (c.f. Eq. (3)):

$$g = e^{i\phi} \left( -(\Delta + \dot{\phi}) \tan(\theta) + i\dot{\theta} \right), \quad (6)$$

where  $\theta$  and  $\phi$  can in principle be chosen arbitrarily provided  $\hat{U} = \mathbb{1}$  at the beginning and the end of the drive. To be consistent with the perturbative solution, we set  $\theta = \arctan(-|\tilde{g}|/\Delta)$  and define  $\phi$  as the complex phase of the coupling, i.e.,  $\tilde{g} = e^{i\phi}|\tilde{g}|$ . We note that, in general,  $\Delta$  could also depend on  $g$  and Eq. (6) becomes an implicit equation for  $g$  instead of a closed-form expression. To obtain an expression for the drive strength  $\Omega$ , one needs to invert the dependence of  $g = f(\Omega)$ , e.g. for  $g = \kappa\Omega$  (and  $\tilde{g} = \kappa\tilde{\Omega}$ ) we get

$$\Omega = \mathcal{F}_\Delta^{(1),G}(\tilde{\Omega}) := \frac{\Delta + \dot{\phi}\tilde{\Omega}}{\Delta} \tilde{\Omega} + \frac{ie^{i\phi}\tilde{\Omega}}{\kappa} \frac{d}{dt} \arctan\left(-\frac{|\kappa\tilde{\Omega}|}{\Delta}\right) \quad (7)$$

with  $e^{i\phi_{\tilde{\Omega}}} = \tilde{\Omega}/|\tilde{\Omega}|$ .

Generalizing to larger Hilbert spaces, we now study the dominant error transitions on the control transmon anharmonic oscillator, where [48]

$$\hat{H} = \frac{\Omega_{\text{CR}}}{2}(\sigma_{01}^+ + \lambda\sigma_{12}^+) + h.c. + \Delta_{10}\hat{\Pi}_1 + (\Delta_{10} + \Delta_{21})\hat{\Pi}_2, \quad (8)$$

with  $\lambda$  the relative coupling strength of the second transition. For detuning  $\Delta_{10}=0$ , the pulse is on resonance and implements a single-qubit gate; however, when  $\Delta_{10}$  is set to the energy difference between the control and the target qubit, a CR operation is activated. To the leading order perturbation, the coupling strength is proportional to  $\Omega_{\text{CR}}$  [23]. An ideal CR pulse generates rotations on the target qubit depending on the control qubit state while leaving the latter intact. This approximation holds well as long as the dressing of the qubit is perturbative. Therefore, we aim at finding a pulse  $\Omega_{\text{CR}}$  with non-zero real integral but introducing no population transfer among any of the three levels of the control qubit. This model, Eq. (8), includes both the leakage error and population flipping on the control qubit [21].

Typically, a CR pulse consists of a rising, a holding and a lowering period, during which the pulse is turned on from zero to the maximum, held for a while and then turned off. We choose the rising portion of the pulse to be

$$\Omega^{(m)}(t) = \Omega_{\text{max}}\mathcal{I}_0 \int_0^t dt' \sin^m\left(\frac{\pi t'}{2t_r}\right), \quad 0 \leq t \leq t_r \quad (9)$$

with the normalization  $\mathcal{I}_0$  fixed via  $\Omega^{(m)}(t_r) = \Omega_{\text{max}}$ . This definition ensures that the pulse is  $m$  times differentiable and the derivatives are 0 at  $t = 0$  and  $t = t_r$ , which guarantees the validity of the frame transformation  $\hat{U}$  introduced above. After the holding time, the lowering phase takes the conjugated and reversed shape. An example of the CR pulse is shown in Fig. 1c. For  $m = 1$  and with zero holding time, the pulse is the same as the widely used Hann window.

Starting from these trigonometric pulses, we first remove the two transitions between states  $|0\rangle \leftrightarrow |1\rangle$  and  $|1\rangle \leftrightarrow |2\rangle$ . We perform a sequential diagonalization of the two couplings, corresponding to applying either Eq. (4) or Eq. (7) twice to the drive shape  $\Omega$ , with  $n = 1$ . While the perturbative expression [Eq. (4)] has a simpler form, Eq. (7) derived from exactly diagonalizing the two-level transitions shows a much lower residual transition rate, especially with small qubit-qubit detuning, which is used in experiments to speed up gates [19].

These two transformations, however, generate an additional effective two-photon coupling between  $|0\rangle$  and  $|2\rangle$ , which is non-negligible in experimentally relevant regimes [20]. Therefore, we need a third correction targeting at this coupling, with  $n = 2$ . As a result, we

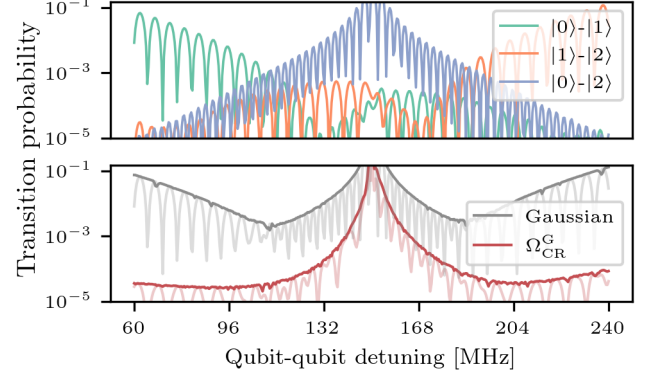


FIG. 2. **Top:** The transition probability among the 3 levels of the control transmon introduced by the CR drive using a flat-top Gaussian pulse with  $t_r = 2\sigma$ . **Bottom:** The total transition error for different pulse schemes. We plot the envelope of the oscillation by taking the maximum over different pulse lengths with the ramping time  $t_r$  fixed. Parameters used are  $\Omega_{\text{max}}/2\pi = 30$  MHz,  $(\Delta_{21} - \Delta_{10})/2\pi = -300$  MHz,  $\lambda = \sqrt{2}$ , and  $t_r = 10$  ns.

obtain the following composed substitution

$$\Omega_{\text{CR}}^P = \mathcal{F}_{\Delta_{21}}^{(1)} \circ \mathcal{F}_{\Delta_{10}}^{(1)} \circ \mathcal{F}_{\Delta_{10} + \Delta_{21}}^{(2)}(\Omega) \quad (10)$$

using the perturbative substitution Eq. (4) or

$$\Omega_{\text{CR}}^G = \mathcal{F}_{\Delta_{21}}^{(1),G} \circ \mathcal{F}_{\Delta_{10}}^{(1),G} \circ \mathcal{F}_{\Delta_{10} + \Delta_{21}}^{(2)}(\Omega) \quad (11)$$

using the exact expression Eq. (7) for the two single-photon transitions. An example of the derived CR pulse is shown in Fig. 1c and a detailed derivation is presented in the supplemental material [49].

To verify the performance of the error suppression, we numerically simulate the dynamics of the three-level Hamiltonian in Eq. (8) and the result is shown in Fig. 2. First, we plot the contribution of the three transition errors for an uncorrected pulse, across the typical experimentally relevant qubit-qubit detuning values. It is clearly illustrated in the plot that all three transitions need to be considered for a sufficient suppression of the errors. Moreover, we observe that partial suppression of the errors (using only one or two  $\mathcal{F}$ ) may increase the unsuppressed ones (see supplemental material [49]), causing them to become nonnegligible even if they were previously small. Next, we compare the total transition error introduced by different pulse schemes. As a baseline, we plot the errors for the flat-top Gaussian pulse, which is commonly used in IBM quantum devices [50]. The DRAG pulse we derived,  $\Omega_{\text{CR}}^G$ , suppresses the error by several orders of magnitude, as long as the drive is not resonant with the two-photon transition. In the supplemental material [49], we also show how each substitution  $\mathcal{F}$  affects the transition probabilities and make a comparison between  $\Omega_{\text{CR}}^P$  and  $\Omega_{\text{CR}}^G$ .

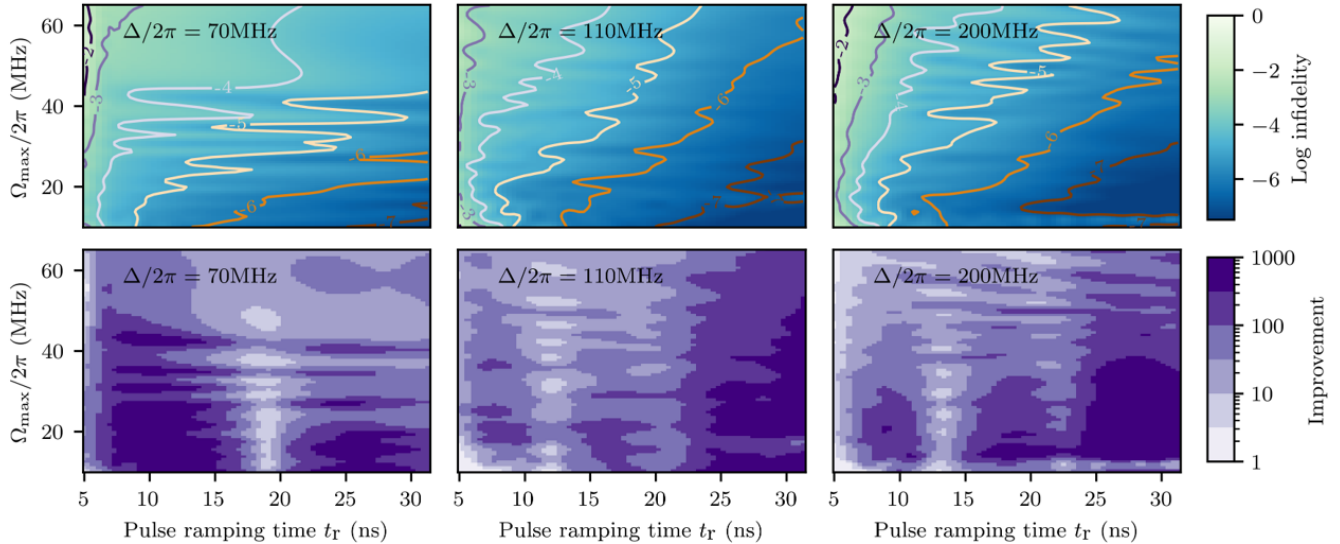


FIG. 3. Infidelities of the CR operations using the derived composite DRAG pulse ( $\Omega_{\text{CR}}^G$ ) with corrections of the rotation-axis error and the improvement compared to the flat-top Gaussian pulse. See Fig. 1c for a schematic pulse shape. All the pulses are closed-form and computed deterministically without numerical calibration. The simulation is repeated for 3 different values of the qubit-qubit detuning with other parameters listed in the supplemental material [49].

*Suppressing multi-qubit rotation-axis error* – A second major part of the error comes from the remaining dynamical operators that do not commute with the ideal dynamics  $ZX$  in the two-qubit subspace. We refer to these as rotation-axis errors for the CR gate, including  $IY$ ,  $IZ$ ,  $ZZ$  and  $ZY$  operators. An overview of the rotation-axis errors and the transformations used below to remove them is shown in Fig. 1d.

First, we remove the  $ZY$  dynamics, which is introduced by the imaginary part of the CR drive, similar to the  $Y$  error in the single-qubit DRAG pulse [51]. We use the transformation

$$\hat{U}_{ZY}(t) = \exp \left[ \int_0^t i\Omega_{ZY}(t') \hat{Z} \hat{Y} dt' \right], \quad (12)$$

where  $\Omega_{ZY}$  denotes the strength of the  $ZY$  Hamiltonian component. Note that because of the symmetry of the CR pulse (see Fig. 1c), the integral is zero at the end of the gate, i.e.,  $\hat{U}_{ZY}(1) = \hat{U}_{ZY}(T) = \mathbb{1}$ . Therefore this frame transformation does not change the final unitary evolution. The derivative part of the transformation,  $i\dot{\hat{U}}_{ZY}\hat{U}_{ZY}^\dagger$ , exactly cancels the existing  $ZY$  Hamiltonian component [52]. In this way, we effectively transform the  $ZY$  error to  $ZZ$  and  $IZ$  errors and slightly modify the strength of the target dynamics  $ZX$ . This transformation can be thought of as a continuous transformation between different gates belonging to the same entanglement class [53]. At the same time, they form a multi-operator generalization to the phase ramping technique in NMR, which itself generalizes static virtual Z gates in circuit QED and ions [54, 55].

Next, we focus on the  $ZZ$  error. The  $ZZ$  error considered here is the dynamical  $ZZ$  error originating from the frame transformation  $\hat{U}$  of the control qubit (i.e. A.C. Stark shifts) and the transformation  $\hat{U}_{ZY}$ . In previous studies, its value is often computed under the least action condition, i.e., the frame transformation should be as close as possible to identity [23, 56]. Here, we break this convention and use pulse shaping to fully compensate for the  $ZZ$  error. Recall that the  $ZZ$  and  $ZX$  are related by a rotation generated by  $IY$ . Hence, we define the transformation

$$\hat{U}_{ZZ} = \hat{I} \otimes \exp \left( -i\beta(t) \hat{Y}/2 \right) \quad (13)$$

with  $\beta = \arctan \left( \frac{\Omega_{zz}}{\Omega_{zx}} \right) \approx \frac{\Omega_{zz}}{\Omega_{zx}}$ . This transformation results in an *enhanced*  $ZX$  strength  $\sqrt{\Omega_{zx}^2 + \Omega_{zz}^2}$  and an additional single-qubit term  $\beta \hat{I} \hat{Y}/2$  to be compensated by a  $Y$  drive on the target qubit. Notice that all previous transformations commute with the  $IY$  drive. Therefore the  $IY$  control remains almost intact in this effective frame, up to the dressing of the qubits.

Finally, the only untreated error, the  $IZ$  component, is compensated for by detuning the CR drive. In general, the exact cancellation of the  $IZ$  error requires time-dependent detuning, i.e., a chirped pulse or phase ramping. Here, as the  $IZ$  term is usually small, we simply compute the total accumulated phase on the target qubit and adjust the constant detuning to compensate for it.

*Numerical simulation* – To verify the performance of the proposed CR drive, we perform full numerical simulations of the two transmons. As we focus on the removal

of dynamical errors of an imperfect CR operation, we choose an architecture where the static  $ZZ$  error is engineered by design to be zero. In particular, we use the QuaDISQ regime [47, 57], where two qubits are coupled through a resonator and the qubit resonator detuning is somewhat smaller than for the typical strong dispersive regime. In the QuaDISQ regime, the virtual interaction with the second excited resonator state cancels the  $ZZ$  interaction caused by the second excited states. The effective coupling strength of  $ZX$  and  $ZZ$  are computed using the non-perturbative analytical diagonalization (NPAD) method [47]. Other approaches can also be used to achieve this, such as adding a direct coupling between the qubits [27, 58] or using off-resonant microwave drives [33, 34]. They have only a small influence on CR drive shape as the qubits are only perturbatively dressed.

In the simulation, we use the analytical pulse shape derived above, without any further optimization or fitting parameters. For simplicity, we ignore the contribution of the (commuting) single-qubit corrections  $ZI$  and  $IX$  and focus only on the equivalent CR unitary. To demonstrate the applicability of the derived pulse to a large range of different drive strengths and ramping speeds, we perform a sweep for different  $\Omega_{\max}$  and  $t_r$  while also varying the qubit-qubit detuning  $\Delta/2\pi=\{70, 80, 200\}$  MHz in the straddling regime. We compute the infidelity using both the derived composite DRAG scheme  $\Omega_{\text{CR}}^G$  with rotation-axis correction and the flat-top Gaussian pulse. Fig. 3 shows a drastic reduction in the coherent error in all regimes via our approach, with 1-3 orders of magnitude improvements similarly seen for the three detunings.

We emphasize again that no numerical calibration is used in the calculation. More details of the numerical simulation are presented in the supplemental material [49]. In addition, we observe that the transition error is barely affected by the drift of the drive strength and is also relatively robust against frequency drift. The improvement still remains under large frequency drift of the qubits, e.g. a 10% deviation of the detuning may increase the transition error by one order of magnitude (see supplemental material [49]), while typical detuning drifts smaller than 1% would barely be noticeable.

*Conclusions* – We presented analytical expressions for driving the CR interaction for superconducting qubits with no unwanted transitions on the control qubit and no unwanted multi-qubit operators. For this approach, we generalized the DRAG formalism to work with a simple composite structure that suppresses multiple error transitions in parallel. At the same time, we derived a completely novel approach for removing multi-operator error, consisting of time-dependently transforming the error terms into the desired entangling form. This resulted in 1-3 orders of magnitude suppression in coherent error when simulating across the range of typical c-QED regimes. Both of these analytical approaches are very general, and can be applied to a wide range of systems,

including other entangling gates in c-QED [59–61] and other quantum technologies. The simplicity of both approaches allows for simple experimental calibration as is already performed with the CR gate [16, 62].

This work was funded by the Federal Ministry of Education and Research (BMBF) within the framework programme "Quantum technologies – from basic research to market" (Project QSolid, Grant No. 13N16149), by the Deutsche Forschungsgemeinschaft (DFG, German Research Foundation) under Germany's Excellence Strategy – Cluster of Excellence Matter and Light for Quantum Computing (ML4Q) EXC 2004/1 – 390534769.

---

\* b.li@fz-juelich.de

† f.motzoi@fz-juelich.de

- [1] Y. Zhao, Y. Ye, H.-L. Huang, Y. Zhang, D. Wu, H. Guan, Q. Zhu, Z. Wei, T. He, S. Cao, F. Chen, T.-H. Chung, H. Deng, D. Fan, M. Gong, C. Guo, S. Guo, L. Han, N. Li, S. Li, Y. Li, F. Liang, J. Lin, H. Qian, H. Rong, H. Su, L. Sun, S. Wang, Y. Wu, Y. Xu, C. Ying, J. Yu, C. Zha, K. Zhang, Y.-H. Huo, C.-Y. Lu, C.-Z. Peng, X. Zhu, and J.-W. Pan, Realization of an Error-Correcting Surface Code with Superconducting Qubits, *Physical Review Letters* **129**, 030501 (2022).
- [2] Google Quantum AI, Suppressing quantum errors by scaling a surface code logical qubit, *Nature* **614**, 676 (2023).
- [3] K. J. Satzinger, Y.-J. Liu, A. Smith, C. Knapp, M. Newman, C. Jones, Z. Chen, C. Quintana, X. Mi, A. Dunsworth, C. Gidney, I. Aleiner, F. Arute, K. Arya, J. Atalaya, *et al.*, Realizing topologically ordered states on a quantum processor, *Science* 10.1126/science.abi8378 (2021).
- [4] Google Quantum AI and Collaborators, Observation of non-Abelian exchange statistics on a superconducting processor (2022), arxiv:arXiv:2210.10255.
- [5] J. Koch, T. M. Yu, J. Gambetta, A. A. Houck, D. I. Schuster, J. Majer, A. Blais, M. H. Devoret, S. M. Girvin, and R. J. Schoelkopf, Charge-insensitive qubit design derived from the Cooper pair box, *Physical Review A* **76**, 042319 (2007).
- [6] C. Rigetti and M. Devoret, Fully microwave-tunable universal gates in superconducting qubits with linear couplings and fixed transition frequencies, *Physical Review B* **81**, 134507 (2010).
- [7] D. Willsch, M. Nocon, F. Jin, H. De Raedt, and K. Michielsen, Gate-error analysis in simulations of quantum computers with transmon qubits, *Physical Review A* **96**, 062302 (2017).
- [8] J. Ghosh, A. G. Fowler, J. M. Martinis, and M. R. Geller, Understanding the effects of leakage in superconducting quantum-error-detection circuits, *Physical Review A* **88**, 062329 (2013).
- [9] M. McEwen, D. Kafri, Z. Chen, J. Atalaya, K. J. Satzinger, C. Quintana, P. V. Klimov, D. Sank, C. Gidney, A. G. Fowler, Y. Chen, V. N. Smelyanskiy, J. M. Martinis, H. Neven, J. Kelly, A. N. Korotkov, A. G. Petukhov, R. Barends, *et al.*, Removing leakage-induced correlated errors in superconducting quantum error cor-

rection, *Nature Communications* **12**, 1761 (2021).

[10] K. C. Miao, M. McEwen, J. Atalaya, D. Kafri, L. P. Pryadko, A. Bengtsson, A. Opremcak, K. J. Satzinger, Z. Chen, P. V. Klimov, C. Quintana, H. Neven, V. Smelyanskiy, A. Petukhov, A. N. Korotkov, D. Sank, Y. Chen, *et al.*, Overcoming leakage in scalable quantum error correction (2022), arxiv:arXiv:2211.04728.

[11] B. M. Varbanov, F. Battistel, B. M. Tarasinski, V. P. Ostroukh, T. E. O'Brien, L. DiCarlo, and B. M. Terhal, Leakage detection for a transmon-based surface code, *npj Quantum Information* **6**, 1 (2020).

[12] C. C. Bultink, T. E. O'Brien, R. Vollmer, N. Muthusubramanian, M. W. Beekman, M. A. Rol, X. Fu, B. Tarasinski, V. Ostroukh, B. Varbanov, A. Bruno, and L. DiCarlo, Protecting quantum entanglement from leakage and qubit errors via repetitive parity measurements, *Science Advances* **6**, eaay3050 (2020).

[13] G. S. Paraoanu, Microwave-induced coupling of superconducting qubits, *Physical Review B* **74**, 140504(R) (2006).

[14] P. C. de Groot, J. Lisenfeld, R. N. Schouten, S. Ashhab, A. Lupaşcu, C. J. P. M. Harmans, and J. E. Mooij, Selective darkening of degenerate transitions demonstrated with two superconducting quantum bits, *Nature Physics* **6**, 763 (2010).

[15] J. M. Chow, A. D. Córcoles, J. M. Gambetta, C. Rigetti, B. R. Johnson, J. A. Smolin, J. R. Rozen, G. A. Keefe, M. B. Rothwell, M. B. Ketchen, and M. Steffen, Simple All-Microwave Entangling Gate for Fixed-Frequency Superconducting Qubits, *Physical Review Letters* **107**, 080502 (2011).

[16] S. Sheldon, E. Magesan, J. M. Chow, and J. M. Gambetta, Procedure for systematically tuning up crosstalk in the cross-resonance gate, *Physical Review A* **93**, 060302(R) (2016).

[17] M. Takita, A. D. Córcoles, E. Magesan, B. Abdo, M. Brink, A. Cross, J. M. Chow, and J. M. Gambetta, Demonstration of Weight-Four Parity Measurements in the Surface Code Architecture, *Physical Review Letters* **117**, 210505 (2016).

[18] M. Takita, A. W. Cross, A. D. Córcoles, J. M. Chow, and J. M. Gambetta, Experimental Demonstration of Fault-Tolerant State Preparation with Superconducting Qubits, *Physical Review Letters* **119**, 180501 (2017).

[19] A. Kandala, K. X. Wei, S. Srinivasan, E. Magesan, S. Carnevale, G. A. Keefe, D. Klaus, O. Dial, and D. C. McKay, Demonstration of a High-Fidelity CNOT Gate for Fixed-Frequency Transmons with Engineered ZZ Suppression, *Physical Review Letters* **127**, 130501 (2021).

[20] M. Malekakhlagh and E. Magesan, Mitigating off-resonant error in the cross-resonance gate, *Physical Review A* **105**, 012602 (2022).

[21] V. Tripathi, M. Khezri, and A. N. Korotkov, Operation and intrinsic error budget of a two-qubit cross-resonance gate, *Physical Review A* **100**, 012301 (2019).

[22] K. X. Wei, E. Pritchett, D. M. Zajac, D. C. McKay, and S. Merkel, Characterizing non-Markovian Off-Resonant Errors in Quantum Gates (2023), arxiv:arXiv:2302.10881.

[23] E. Magesan and J. M. Gambetta, Effective Hamiltonian models of the cross-resonance gate, *Physical Review A* **101**, 052308 (2020).

[24] M. Malekakhlagh, E. Magesan, and D. C. McKay, First-principles analysis of cross-resonance gate operation, *Physical Review A* **102**, 042605 (2020).

[25] N. Sundaresan, I. Lauer, E. Pritchett, E. Magesan, P. Jurcevic, and J. M. Gambetta, Reducing Unitary and Spectator Errors in Cross Resonance with Optimized Rotary Echoes, *PRX Quantum* **1**, 020318 (2020).

[26] P. Jurcevic, A. Javadi-Abhari, L. S. Bishop, I. Lauer, O. E. Dial, J. M. Chow, J. M. Gambetta, *et al.*, Demonstration of quantum volume 64 on a superconducting quantum computing system, *Quantum Science and Technology* **6**, 025020 (2021).

[27] P. Mundada, G. Zhang, T. Hazard, and A. Houck, Suppression of Qubit Crosstalk in a Tunable Coupling Superconducting Circuit, *Physical Review Applied* **12**, 054023 (2019).

[28] X. Xu and M. Ansari, Parasitic-Free Gate: An Error-Protected Cross-Resonance Switch in Weakly Tunable Architectures, *Physical Review Applied* **19**, 024057 (2023).

[29] F. Motzoi, J. M. Gambetta, P. Rebentrost, and F. K. Wilhelm, Simple Pulses for Elimination of Leakage in Weakly Nonlinear Qubits, *Physical Review Letters* **103**, 110501 (2009).

[30] J. M. Gambetta, F. Motzoi, S. T. Merkel, and F. K. Wilhelm, Analytic control methods for high-fidelity unitary operations in a weakly nonlinear oscillator, *Physical Review A* **83**, 012308 (2011).

[31] F. Motzoi and F. K. Wilhelm, Improving frequency selection of driven pulses using derivative-based transition suppression, *Physical Review A* **88**, 062318 (2013).

[32] L. S. Theis, F. Motzoi, S. Machnes, and F. K. Wilhelm, Counteracting systems of diabaticities using DRAG controls: The status after 10 years, *EPL (Europhysics Letters)* **123**, 60001 (2018).

[33] B. K. Mitchell, R. K. Naik, A. Morvan, A. Hashim, J. M. Kreikebaum, B. Marinelli, W. Lavrijsen, K. Nowrouzi, D. I. Santiago, and I. Siddiqi, Hardware-Efficient Microwave-Activated Tunable Coupling between Superconducting Qubits, *Physical Review Letters* **127**, 200502 (2021).

[34] K. X. Wei, E. Magesan, I. Lauer, S. Srinivasan, D. F. Bogorin, S. Carnevale, G. A. Keefe, Y. Kim, D. Klaus, W. Landers, N. Sundaresan, C. Wang, E. J. Zhang, M. Steffen, O. E. Dial, D. C. McKay, and A. Kandala, Hamiltonian Engineering with Multicolor Drives for Fast Entangling Gates and Quantum Crosstalk Cancellation, *Physical Review Letters* **129**, 060501 (2022).

[35] Y. Kim, A. Morvan, L. B. Nguyen, R. K. Naik, C. Jünger, L. Chen, J. M. Kreikebaum, D. I. Santiago, and I. Siddiqi, High-fidelity three-qubit iToffoli gate for fixed-frequency superconducting qubits, *Nature Physics* 10.1038/s41567-022-01590-3 (2022).

[36] N. Goss, A. Morvan, B. Marinelli, B. K. Mitchell, L. B. Nguyen, R. K. Naik, L. Chen, C. Jünger, J. M. Kreikebaum, D. I. Santiago, J. J. Wallman, and I. Siddiqi, High-fidelity qutrit entangling gates for superconducting circuits, *Nature Communications* **13**, 7481 (2022).

[37] P. Zhao, K. Linghu, Z. Li, P. Xu, R. Wang, G. Xue, Y. Jin, and H. Yu, Quantum Crosstalk Analysis for Simultaneous Gate Operations on Superconducting Qubits, *PRX Quantum* **3**, 020301 (2022).

[38] T. Q. Cai, X. Y. Han, Y. K. Wu, Y.-L. Ma, J. H. Eberly, Z. L. Wang, H. Y. Zhang, H. Y. Wang, Y. P. Song, and L. M. Duan, Impact of Spectators on a Two-Qubit Gate in a Tunable Coupling Superconducting Circuit, *Physical*

Review Letters **127**, 060505 (2021).

[39] J. F. Marques, H. Ali, B. M. Varbanov, M. Finkel, H. M. Veen, S. L. M. van der Meer, S. Valles-Sanclemente, N. Muthusubramanian, M. Beekman, N. Haider, B. M. Terhal, and L. DiCarlo, All-microwave leakage reduction units for quantum error correction with superconducting transmon qubits (2023), arxiv:arXiv:2302.09876.

[40] S. Kirchhoff, T. Kekler, P. J. Liebermann, E. Assémat, S. Machnes, F. Motzoi, and F. K. Wilhelm, Optimized cross-resonance gate for coupled transmon systems, *Physical Review A* **97**, 042348 (2018).

[41] M. Dalgaard, F. Motzoi, J. J. Sørensen, and J. Sherson, Global optimization of quantum dynamics with AlphaZero deep exploration, *npj Quantum Information* **6**, 1 (2020).

[42] Y. Baum, M. Amico, S. Howell, M. Hush, M. Liuzzi, P. Mundada, T. Merkh, A. R. R. Carvalho, and M. J. Biercuk, Experimental Deep Reinforcement Learning for Error-Robust Gate-Set Design on a Superconducting Quantum Computer, *PRX Quantum* **2**, 040324 (2021).

[43] R. Unanyan, L. Yatsenko, K. Bergmann, and B. Shore, Laser-induced adiabatic atomic reorientation with control of diabatic losses, *Optics Communications* **139**, 48 (1997).

[44] M. Demirplak and S. A. Rice, Adiabatic Population Transfer with Control Fields, *The Journal of Physical Chemistry A* **107**, 9937 (2003).

[45] X. Chen, I. Lizuain, A. Ruschhaupt, D. Guéry-Odelin, and J. G. Muga, Shortcut to Adiabatic Passage in Two- and Three-Level Atoms, *Physical Review Letters* **105**, 123003 (2010).

[46] D. Guéry-Odelin, A. Ruschhaupt, A. Kiely, E. Torrontegui, S. Martínez-Garaot, and J. G. Muga, Shortcuts to adiabaticity: Concepts, methods, and applications, *Reviews of Modern Physics* **91**, 045001 (2019).

[47] B. Li, T. Calarco, and F. Motzoi, Nonperturbative Analytical Diagonalization of Hamiltonians with Application to Circuit QED, *PRX Quantum* **3**, 030313 (2022).

[48] Although the Hamiltonian looks similar to the  $\Lambda$  system often studied in the STIRAP problem, it has two differences. First, none of the three levels is close to degeneracy, which complicates the diagonalization. Second, instead of only isolating a single dark state from the rest two, all the transitions among the three levels need to be suppressed.

[49] See Supplemental Material for derivation of the recursive formula, details on the numerical simulation and the robustness study of the CR drive.

[50] IBM Quantum (2021).

[51] Z. Chen, J. Kelly, C. Quintana, R. Barends, A. N. Korotkov, J. M. Martinis, *et al.*, Measuring and Suppressing Quantum State Leakage in a Superconducting Qubit, *Physical Review Letters* **116**, 020501 (2016).

[52] Note that this corresponds to an interaction picture with respect to the unwanted term, effectively transforming the error into the other operators in the Hamiltonian.

[53] J. Zhang, J. Vala, S. Sastry, and K. B. Whaley, Minimum Construction of Two-Qubit Quantum Operations, *Physical Review Letters* **93**, 020502 (2004).

[54] S. L. Patt, Single- and multiple-frequency-shifted laminar pulses, *Journal of Magnetic Resonance* (1969) **96**, 94 (1992).

[55] D. C. McKay, C. J. Wood, S. Sheldon, J. M. Chow, and J. M. Gambetta, Efficient Z gates for quantum computing, *Physical Review A* **96**, 022330 (2017).

[56] X. Xu and M. H. Ansari, ZZ freedom in two qubit gates, *Physical Review Applied* **15**, 064074 (2021).

[57] M. H. Goerz, F. Motzoi, K. B. Whaley, and C. P. Koch, Charting the circuit QED design landscape using optimal control theory, *npj Quantum Information* **3**, 37 (2017).

[58] Y. Xu, J. Chu, J. Yuan, J. Qiu, Y. Zhou, L. Zhang, X. Tan, Y. Yu, S. Liu, J. Li, F. Yan, and D. Yu, High-fidelity, high-scalability two-qubit gate scheme for superconducting qubits, *Physical Review Letters* **125**, 240503 (2020).

[59] K. N. Nesterov, C. Wang, V. E. Manucharyan, and M. G. Vavilov, CNOT Gates for Fluxonium Qubits via Selective Darkening of Transitions, *Physical Review Applied* **18**, 034063 (2022).

[60] E. Dogan, D. Rosenstock, L. L. Guevel, H. Xiong, R. A. Mencia, A. Somoroff, K. N. Nesterov, M. G. Vavilov, V. E. Manucharyan, and C. Wang, Demonstration of the Two-Fluxonium Cross-Resonance Gate (2022), arxiv:arXiv:2204.11829.

[61] Q. Ficheux, L. B. Nguyen, A. Somoroff, H. Xiong, K. N. Nesterov, M. G. Vavilov, and V. E. Manucharyan, Fast Logic with Slow Qubits: Microwave-Activated Controlled-Z Gate on Low-Frequency Fluxoniums, *Physical Review X* **11**, 021026 (2021).

[62] A. D. Patterson, J. Rahamim, T. Tsunoda, P. A. Spring, S. Jebari, K. Ratter, M. Mergenthaler, G. Tancredi, B. Vlastakis, M. Esposito, and P. J. Leek, Calibration of a Cross-Resonance Two-Qubit Gate Between Directly Coupled Transmons, *Physical Review Applied* **12**, 064013 (2019).

[63] L. H. Pedersen, N. M. Møller, and K. Mølmer, Fidelity of quantum operations, *Physics Letters A* **367**, 47 (2007).

## Supplementary material for "Suppression of coherent errors in Cross-Resonance gates via recursive DRAG"

### I. DERIVATION OF THE SUBSTITUTION RULES AND THE EFFECTIVE HAMILTONIAN FOR THE CONTROL QUBIT

In the following, we show the derivation of the substitution rule of  $\Omega$  in the main text via Schrieffer Wolff perturbation. We use the three-level Hamiltonian to represent the control qubit

$$\hat{H}_0 = \frac{\epsilon\Omega_{\text{CR}}}{2}(\hat{\sigma}_{01}^+ + \lambda\hat{\sigma}_{12}^+) + h.c. + \Delta_{10}\hat{\Pi}_1 + (\Delta_{10} + \Delta_{21})\hat{\Pi}_2 \quad (\text{S1})$$

where  $\epsilon$  is used to denote the perturbation order. We omit the perturbative corrections to the diagonal part of the Hamiltonian as they have no effect on the leading-order perturbative coupling strength. The derivation includes three steps, each targeting one coupling. The perturbative transformation generated by an anti-hermitian matrix  $\hat{S}$  is defined as

$$\hat{H}' = i\dot{\hat{S}} + \hat{H} + [\hat{S}, \hat{H}] + \frac{1}{2}[\hat{S}, [\hat{S}, \hat{H}]] + \dots \quad (\text{S2})$$

First, we apply the perturbative diagonalization targeting the  $|0\rangle \leftrightarrow |1\rangle$  transition

$$\hat{S}_1 = \frac{\epsilon}{2} \left( \frac{\Omega_1}{\Delta_{10}}\hat{\sigma}_{01}^+ + \frac{\lambda\Omega_1}{\Delta_{10}}\hat{\sigma}_{12}^+ \right) - h.c. \quad (\text{S3})$$

The first component in  $\hat{S}_1$  is chosen to remove the  $|0\rangle \leftrightarrow |1\rangle$  coupling perturbatively. According to the derivation in the main text, we define a substitution for  $\Omega_{\text{CR}}^{\text{P}}$

$$\Omega_{\text{CR}}^{\text{P}} = \Omega_1 - i\frac{\dot{\Omega}_1}{\Delta_{10}}. \quad (\text{S4})$$

The second term in Eq. (S3) is chosen such that  $i\dot{\hat{S}}_1$  is proportional to the  $Y$  control Hamiltonian. This ensures that in the derived effective Hamiltonian, no  $\dot{\Omega}_1$  appears in the  $|1\rangle \leftrightarrow |2\rangle$  coupling, because it is absorbed in  $\Omega_{\text{CR}}$ . Note that it does not diagonalize the  $|1\rangle \leftrightarrow |2\rangle$  coupling, which would need  $\frac{\lambda\Omega_1}{\Delta_{12}}\hat{\sigma}_{12}^+$  instead. As a result, we obtain

$$\hat{H}_1 = \left(1 - \frac{\Delta_{21}}{\Delta_{10}}\right) \left(\frac{1}{2}\lambda\Omega_1\epsilon\hat{\sigma}_{12}^+ - \frac{\lambda\Omega_1^2\epsilon^2}{8\Delta_{10}}\hat{\sigma}_{02}^+\right) + h.c. + \text{diag} + \mathcal{O}(\epsilon^3).$$

In the second step, we perform another perturbative diagonalization that removes the  $|1\rangle \leftrightarrow |2\rangle$  transition:

$$S_2 = \left(1 - \frac{\Delta_{21}}{\Delta_{10}}\right) \frac{\lambda\Omega_2\epsilon}{2\Delta_{21}}\hat{\sigma}_{12}^+ - h.c. \quad (\text{S5})$$

and substitute

$$\Omega_1 = \Omega_2 - i\frac{\dot{\Omega}_2}{\Delta_{21}}. \quad (\text{S6})$$

This gives the effective Hamiltonian

$$\hat{H}_2 = \left(\frac{\Delta_{21}}{\Delta_{10}} - 1\right) \left(\Omega_2 - i\frac{\dot{\Omega}_2}{\Delta_{21}}\right)^2 \frac{\lambda\epsilon^2}{8\Delta_{10}}\hat{\sigma}_{02}^+ + h.c. + \text{diag} + \mathcal{O}(\epsilon^3) \quad (\text{S7})$$

where both single-photon transitions are removed to the leading order.

It may seem strange that the remaining coupling for the  $|0\rangle \leftrightarrow |2\rangle$  transition is not symmetric with respect to the order of the transformations of  $|0\rangle \leftrightarrow |1\rangle$  and  $|1\rangle \leftrightarrow |2\rangle$ , although the two substitutions commute. In fact, we can perform a transformation  $\hat{S}_3$

$$\hat{S}_3 = -\left(\frac{1}{\Delta_{21}} - \frac{1}{\Delta_{10}}\right) \frac{(\lambda\Omega_2^2\epsilon^2)}{8\Delta_{10}}\hat{\sigma}_{02}^+ - h.c. \quad (\text{S8})$$

which only removes the  $\Omega\dot{\Omega}$  term and gives

$$H_3 = \frac{1}{8}\lambda\epsilon^2 \left( \frac{1}{\Delta_{21}} - \frac{1}{\Delta_{10}} \right) \left( \frac{\dot{\Omega}_2^2}{\Delta_{21}\Delta_{10}} + \Omega_2^2 \right) \hat{\sigma}_{02}^+ + h.c. + \text{diag} + \mathcal{O}(\epsilon^3). \quad (\text{S9})$$

Lastly, we perform the third step to suppress the remaining  $|0\rangle \leftrightarrow |2\rangle$  coupling. To fully remove this transition one needs to solve the differential equation

$$\left( \frac{\dot{\Omega}_2^2}{\Delta_{21}\Delta_{10}} + \Omega_2^2 \right) = \left( \frac{\dot{\Omega}_3^2}{\Delta_{21}\Delta_{10}} + \Omega_3^2 \right) - i \frac{d}{dt} \frac{\left( \frac{\dot{\Omega}_3^2}{\Delta_{21}\Delta_{10}} + \Omega_3^2 \right)}{\Delta_{20}}, \quad (\text{S10})$$

which is difficult because of the non-linearity. Moreover, it may result in a pulse that does not fulfil the boundary condition, unless  $\Omega_3$  is carefully chosen to ensure that. For simplicity, we here assume that the pulse ramping is quasi-adiabatic i.e.  $\Omega_2 \gg \frac{\dot{\Omega}_2}{\Delta}$ . In this case, we can ignore the term proportional to  $\dot{\Omega}_2^2$ . We then define the last transformation that diagonalizes the  $|0\rangle \leftrightarrow |2\rangle$  transition

$$\hat{S}_4 = \frac{1}{8}\lambda\epsilon^2 \left( \frac{1}{\Delta_{21}} - \frac{1}{\Delta_{10}} \right) \frac{\Omega_2^2}{\Delta_{20}} \hat{\sigma}_{02}^+ - h.c. \quad (\text{S11})$$

and substitute

$$\Omega_2 = \sqrt{\Omega_3^2 - i \frac{2\Omega_3\dot{\Omega}_3}{\Delta_{20}}}. \quad (\text{S12})$$

As a result, we suppress all three transitions up to  $\mathcal{O}(\epsilon^3) + \mathcal{O}(\dot{\Omega}^2/\Delta^4)$ .

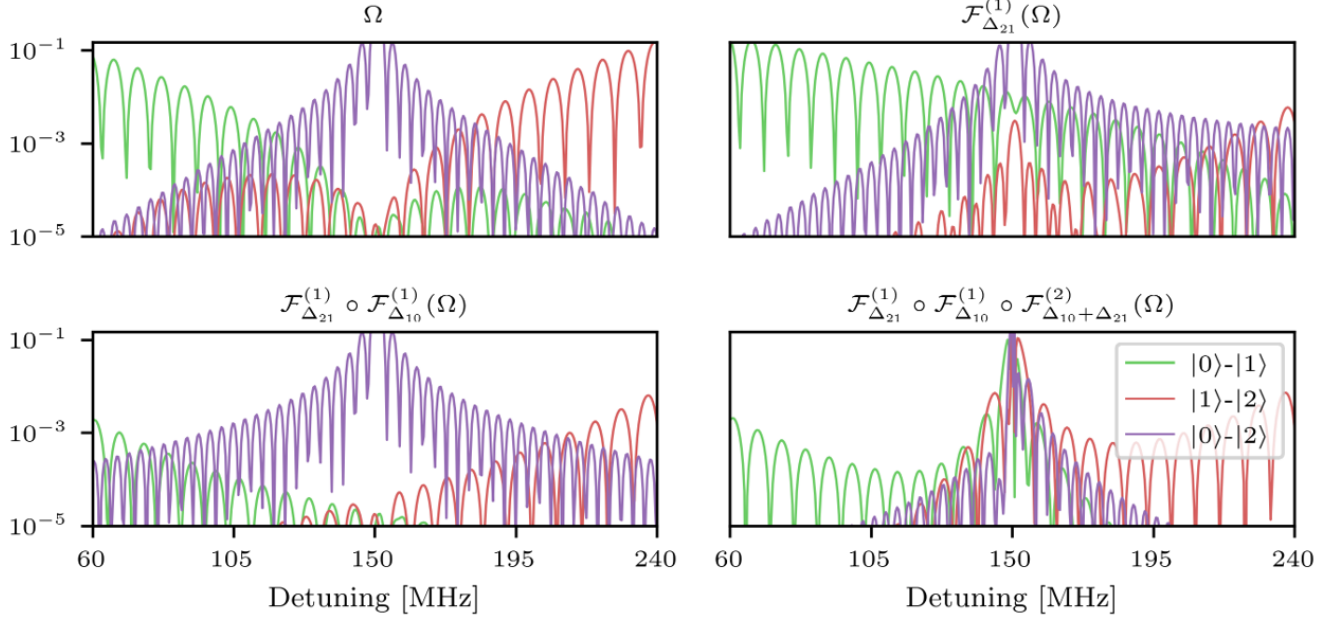


FIG. S1. Transition probabilities using different perturbative pulse substitutions.

## II. COMPARING DIFFERENT PULSE SCHEMES FOR TRANSITION ERROR SUPPRESSION

In Fig. S1, we plot the transition probabilities among the three levels, using different substitutions. One observes the suppression of different transitions by the corresponding pulse substitution. In addition, we see that a solution

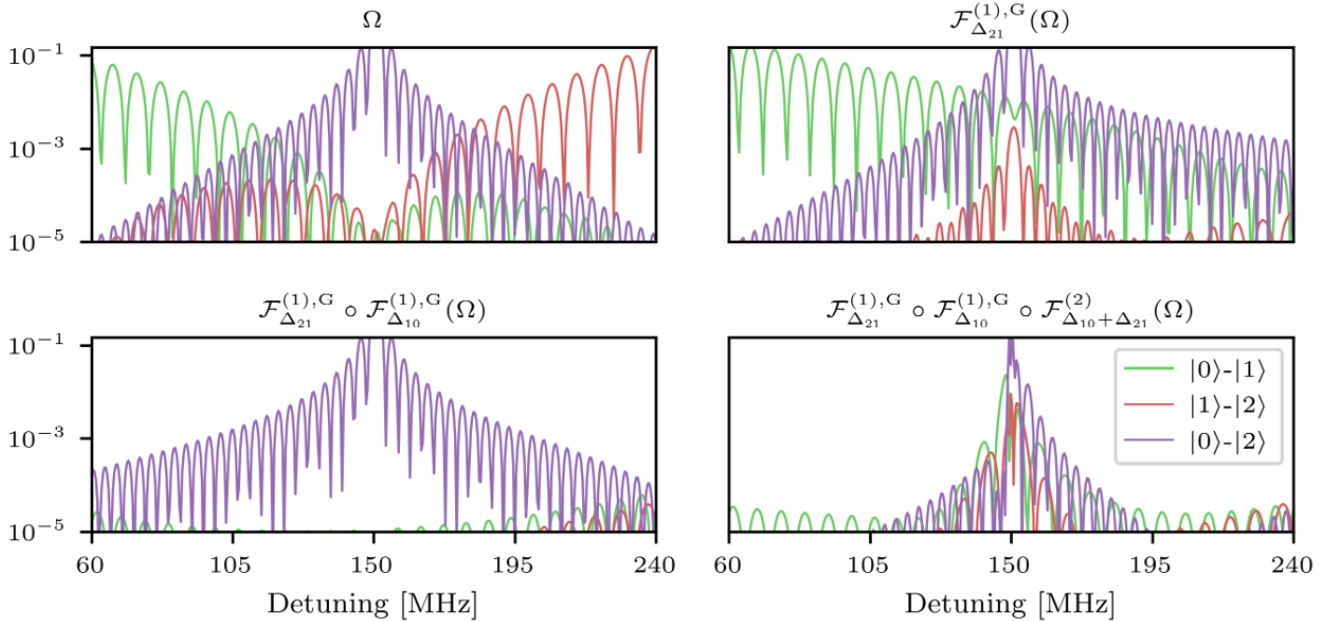


FIG. S2. Transition probabilities using the substitutions derived from the exact two-level diagonalization for the single-photon transitions.

that suppresses only part of the transitions may increase other transitions, which underlines the importance of the simultaneous suppression of all transitions.

It is also evident from Fig. S1 that the leading-order perturbative solution only suppresses the single-photon transitions to  $10^{-3}$ . The transitions are not sufficiently suppressed when the detuning is small or close to the anharmonicity because the ratio between the coupling and the energy gap exceeds the perturbative regime. To improve upon it, we replace the substitutions for the single-photon transitions with the exact diagonalization in the two-level subsystem and obtain Fig. S2. Notice that the substitution  $\mathcal{F}^{(1),G}$  is only exact with respect to the two-level subsystem, perturbative corrections to the energy gaps and other couplings are still ignored. Nonetheless, it still significantly improves the performance compared to the perturbative expressions. Part of the reason is that we are in the straddling regime and usually only one of the  $|0\rangle \leftrightarrow |1\rangle$  or  $|1\rangle \leftrightarrow |2\rangle$  transitions goes beyond the perturbative regime.

To better illustrate the difference between the pulse schemes, we take the sum of the three transitions and the maximum over pulses with various holding lengths. In this way, the oscillation caused by the pulse timing is removed and only the upper envelope remains. Here we plot the three analytical pulse shapes in Fig. S3: the naive  $\Omega^{(1)}$  pulse (of which the rising and falling part is identical to a Hann window), the recursive DRAG pulse derived from perturbation  $\Omega_{\text{CR}}^P$  and from the exact two-level diagonalization  $\Omega_{\text{CR}}^G$ . In addition, we also show the numerically optimized leading-order DRAG scheme  $\Omega^{(1)} - a\dot{\Omega}^{(1)}$ , where the parameter  $a$  is numerically optimized to get the lowest possible total transition error [20]. It is observed that the optimized leading-order DRAG only suppresses the error if one of the single-photon transitions is dominant. In contrast, the analytical recursive DRAG pulse brings better improvement for a much larger range of parameter regimes.

### III. DETAILS ON THE NUMERICAL SIMULATION

In the numerical simulation of the CR gate, we use an effective Duffing model truncated at 4 levels

$$\hat{H}_0 = \omega_a \hat{a}_a^\dagger \hat{a}_a + \sum_{j=1,2} \omega_j \hat{b}_j^\dagger \hat{b}_j + \frac{\alpha_j}{2} \hat{b}_j^\dagger \hat{b}_j^\dagger \hat{b}_j \hat{b}_j + g_j (\hat{b}_j \hat{a}^\dagger + \hat{b}_j^\dagger \hat{a}) \quad (\text{S13})$$

where  $\hat{b}_j$  and  $\hat{a}$  are the annihilation operators for qubit  $j$  and the resonator and  $g_j$  is the coupling strength. Diagonalizing this time-independent Hamiltonian gives us the dressed eigenstates and eigenenergies, which are used for computing the CR pulse shape according to the substitution rules.

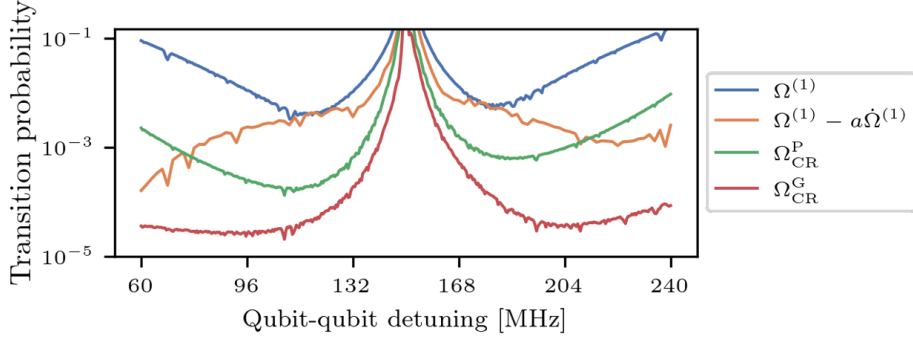


FIG. S3. The total transition error for different pulse schemes. Parameters used are the same as for Fig. 2 in the main text.

The microwave drive on qubit  $j$  is written as

$$\hat{H}_c = \text{Re}(\Omega_{\text{CR}})(e^{-i\omega_d t} \hat{b}_j^\dagger + e^{i\omega_d t} \hat{b}_j) + i \text{Im}(\Omega_{\text{CR}})(e^{-i\omega_d t} \hat{b}_j^\dagger - e^{i\omega_d t} \hat{b}_j) \quad (\text{S14})$$

where  $\omega_d$  is the driving frequency, initially chosen as the frequency of the target qubit. For simplicity, we use the same drive frequency for both the control and the target qubit. By a rotating frame transformation  $\hat{R} = e^{i\hat{H}_R}$  with  $\hat{H}_R = \omega_d(\hat{a}^\dagger \hat{a} + \hat{b}_1^\dagger \hat{b}_1 + \hat{b}_2^\dagger \hat{b}_2)$ , we obtain a Hamiltonian without fast oscillation.

To focus on the dynamical error, we choose the architecture where the static ZZ error is cancelled. In this work, we choose the qubit-resonator-qubit architecture in the QuaDISQ regime, where the virtual interaction with the second excited resonator state cancels the ZZ coupling [47, 57]. The parameters approximately satisfy the equation of a circle  $(\Delta_1 - \Delta_2)^2 + (\Delta_1 + \Delta_2 - \alpha)^2 = \alpha^2$ , where  $\Delta_j = \omega_j - \omega_a$  and the anharmonicities  $\alpha_j$  of the two qubits are assumed to be the same. After the parameters with no static ZZ interaction are determined, the CR pulse is calculated from the drive strength and the dressed qubit frequencies. The gate time, i.e., the holding duration of the pulse, is computed from the effective ZX coupling strength, using the nonperturbative diaognalization [47].

Because we ensure that the dominant dynamics in the effective frame is the ZX dynamics, the two single-qubit corrections,  $ZI$  and  $IX$ , commute with it. Therefore, they can be calibrated separately, independent of the CR drive. We define  $\hat{\mathcal{U}}$  as the unitary operator generated by the time-dependent Hamiltonian, the transition probability between state  $|j\rangle$  and  $|k\rangle$  is given by

$$P_{jk} = |\langle j | \hat{\mathcal{U}} | k \rangle|^2. \quad (\text{S15})$$

Given an ideal unitary  $\hat{\mathcal{U}}_I$  for a two-qubit gate, the average gate fidelity is defined as [63]

$$F[\hat{U}_Q] = \frac{\text{Tr}[\hat{\mathcal{U}}_Q \hat{\mathcal{U}}_Q^\dagger]}{d(d+1)} + \frac{\left| \text{Tr}[\hat{\mathcal{U}}_Q \hat{\mathcal{U}}_I^\dagger] \right|^2}{d(d+1)} \quad (\text{S16})$$

where  $\hat{\mathcal{U}}_Q$  is the full unitary truncated to the two-qubit subspace and  $d = 4$ . Because we ignore the possible single-qubit correction  $ZI$  and  $IX$ , we compute the maximal fidelity optimized over the possible single-qubit rotation angles

$$\tilde{F} = \max_{\{\theta_1, \theta_2\}} F \left[ e^{-i(\theta_1 \hat{I} \hat{X} + \theta_2 \hat{Z} \hat{I})} \hat{U}_Q e^{i(\theta_1 \hat{I} \hat{X} + \theta_2 \hat{Z} \hat{I})} \right]. \quad (\text{S17})$$

We compute the infidelity both using the flat-top Gaussian pulse and the derived DRAG pulse  $\Omega_{\text{CR}}^G$ . The infidelities are shown in Fig. S4. The bottom row of the plots is identical to the upper row of Fig. 3 in the main text, shown here for comparison. The remaining oscillations in the plot for the improved CR pulse indicate the existence of other off-resonant effects. We identify them as entangling transitions between the control and target qubits, such as the SWAP-like transition induced by A.C. Stark shift of the CR drive. They are orders of magnitude smaller than the targeted error terms in this paper and are left for further research. For the simulation, we choose the anharmonicity  $\alpha = -300$  MHz and  $g_j = 30$  MHz. In the QuaDISQ regime, this results in a direct-CNOT time for about 200 ns, excluding single-qubit correction. Using other coupling architectures while keeping the entanglement strength at a similar level, the derived CR pulse will achieve a similar level of improvement.

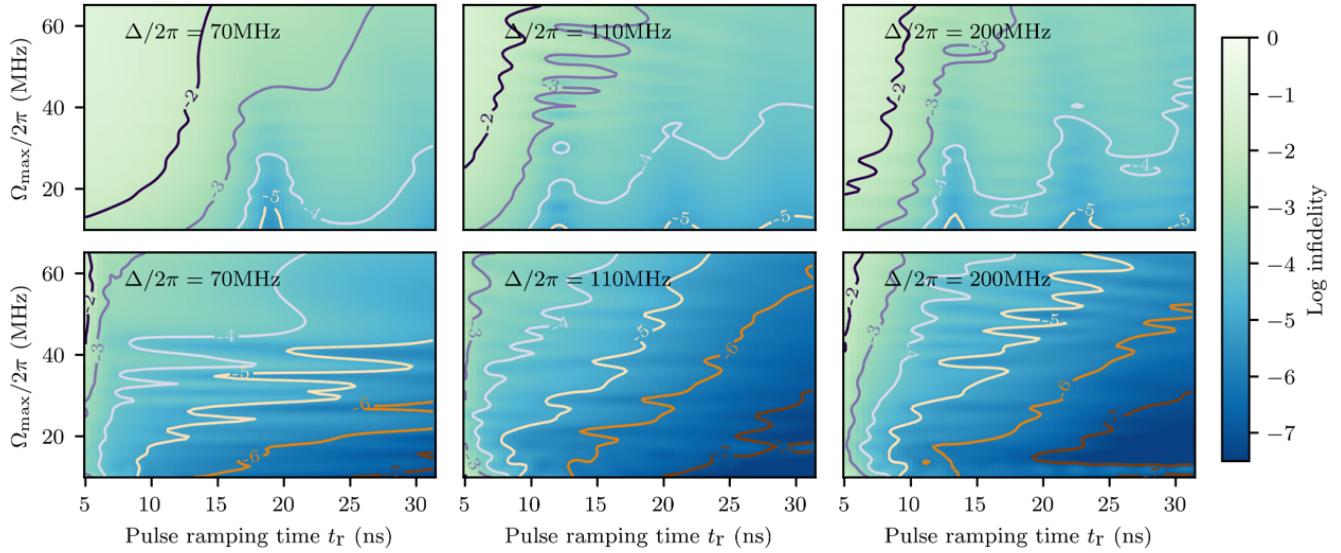


FIG. S4. Comparison of the CR gate infidelity with a flat-top Gaussian pulse (top) and with the improved CR pulse (bottom). All the pulses are computed deterministically without numerical calibration. The simulation is repeated for 3 different values of the qubit-qubit detuning.

#### IV. ROBUSTNESS OF THE CR DRIVE

Superconducting qubits often suffer from the drift of the qubit frequency and the drive strength. In the following, we investigate the performance of the derived analytical pulse shape against those drifts. For simplicity, we assume that the drift is constant during the CR drive. We derive the pulse shape using  $\Omega_{\max}$  and the control qubit frequency  $\Delta_1$  and then perform the full two-qubit simulation using  $\Omega_{\max} + \epsilon_{\Omega}$  and  $\Delta_1 + \epsilon_{\Delta}$ .

The total error transition probability is computed from the unitary evolution and plotted on Fig. S5. The drift of the drive strength causes some oscillations but does not significantly increase the error. This can be qualitatively explained in the two-level derivation. Because the X and Y drives drift simultaneously, the suppression remains the same in the first-order perturbation. Only in the next order does it come into the picture through the correction to the energy gap via Stark shift. The transition error is increased by one order of magnitude if the frequency drifts about 10% with respect to the qubit-qubit detuning. Note that in practice drifts are usually much smaller, in the kHz regime. Not surprisingly, the analytical pulse shape is not located at the region with the absolute lowest error. Therefore, the performance will benefit from further calibration, both in simulation and experiment.

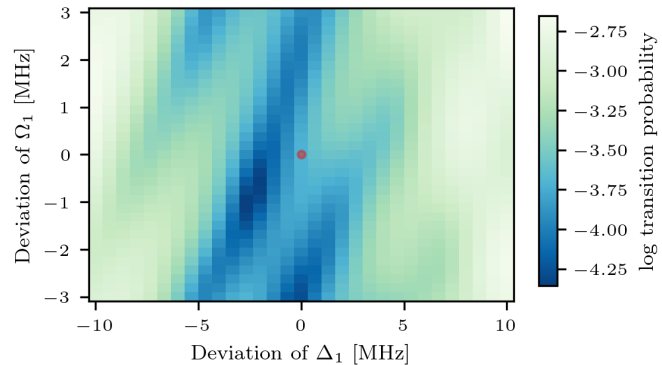


FIG. S5. The total error transition probabilities for a precalculated pulse shape under the effect of parameter drift. The red dot marks the data point that uses the initial parameters:  $\Omega_{\max}/2\pi = 40$  MHz,  $\alpha/2\pi = -300$  MHz,  $\Delta/2\pi = 110$  MHz and  $t_r = 10$  ns.